

# The NFLikelihood: an unsupervised DNNLikelihood from Normalizing Flows

Humberto Reyes-González<sup>1,2,\*</sup> and Riccardo Torre<sup>2,†</sup>

<sup>1</sup> Department of Physics, University of Genova, Via Dodecaneso 33, 16146 Genova, Italy

<sup>2</sup> INFN, Sezione di Genova, Via Dodecaneso 33, I-16146 Genova, Italy

\* humbertoalonso.reyesgonzalez@edu.unige.it

† riccardo.torre@ge.infn.it

## Abstract

We propose the NFLikelihood, an unsupervised version, based on Normalizing Flows, of the DNNLikelihood proposed in Ref. [1]. We show, through realistic examples, how Autoregressive Flows, based on affine and rational quadratic spline bijectors, are able to learn complicated high-dimensional Likelihoods arising in High Energy Physics (HEP) analyses. We focus on a toy LHC analysis example already considered in the literature and on two Effective Field Theory fits of flavor and electroweak observables, whose samples have been obtained through the HEPFit code. We discuss advantages and disadvantages of the unsupervised approach with respect to the supervised one and discuss possible interplays of the two.

## Contents

<b>1</b>	<b>Introduction</b>	<b>2</b>
<b>2</b>	<b>Likelihood functions for LHC analyses</b>	<b>2</b>
2.1	The LHC-like new physics search Likelihood	2
2.2	The ElectroWeak fit Likelihood	3
2.3	The Flavor fit Likelihood	3
<b>3</b>	<b>Evaluation Metrics</b>	<b>3</b>
<b>4</b>	<b>The NFLikelihood</b>	<b>4</b>
4.1	The Toy Likelihood	5
4.2	The EW Likelihood.	6
4.3	Flavor Likelihood	7
<b>5</b>	<b>Conclusion</b>	<b>9</b>
<b>A</b>	<b>Details of the EW and Flavor Likelihoods</b>	<b>12</b>
	<b>References</b>	<b>12</b>

# 1 Introduction

The distribution, preservation, and reinterpretation of experimental and phenomenological Likelihoods arising in High Energy Physics (HEP) and astrophysics is an important and open topic [2]. In Ref. [1] it was shown how deep learning can play a crucial role in this context, by showing how the problem of encoding the Likelihood function into a Deep Neural Network (DNN) can be formulated as a supervised learning problem of regression. In simple terms, the values of the parameters  $\mathbf{x}$  and of the corresponding Likelihood  $y = \mathcal{L}(\mathbf{x})$  are used to train a fully connected multilayer perceptron (MLP), which delivers a “pseudo-analytical” representation of the Likelihood function in terms of a DNN, therefore called DNNLikelihood.

In a recent paper, we have shown that Normalizing Flows (NFs) of the coupling and autoregressive type, are able to perform density estimation of very high dimensional probability density functions (PDFs) with great accuracy and with limited training samples and hyperparameters tuning [3]. Moreover, trained NFs, can be used as sample generators with two different approaches: on the one hand one can draw samples from the base distribution and transform them through the generative direction of the NFs, obtaining samples distributed according to the target PDF; on the other hand, the normalizing direction of the NFs can be used to get a fast prediction of the density for a given sample, allowing one to use the NF to assist and speed up traditional sequential Monte Carlo techniques [4–11].

In this paper we show how Autoregressive Normalizing Flows (ANF) can be used to learn complicated Likelihoods, doing density estimation starting from the  $\mathbf{x}$  samples only and therefore offering an unsupervised approach to the DNNLikelihood.<sup>1</sup> We call the Likelihood encoded by NFs the NFLikelihood. The aim of this paper is twofold: on the one hand we want to give explicit physics examples of the performances of the Autoregressive Flows studied in Ref. [3], which only considered toy distributions based on mixtures of Gaussians and truncated Gaussians; on the other hand we want to propose the NFLikelihood as an alternative DNNLikelihood, discussing advantaged and disadvantages of the unsupervised approach, with respect to the supervised one.

One important remark is that, since we are interested here in discussing the NF performances in learning some physical complicated densities, we focused on learning the posterior probability (not just the Likelihood), since these were the data we had at our disposal. Our approach can of course be trivially extended to the Likelihood by removing the contribution of the (known) prior used to sample the posterior.

The paper is organized as follows. In Section 2 we briefly describe the three phenomenological Likelihoods that we consider. Section 3 contains a discussion of the figures of merit that we used in our analysis, while Section 4 presents the main results. Finally, we report our conclusions in Section 5.

## 2 Likelihood functions for LHC analyses

In this analysis, we consider three Likelihoods of different dimensionality. We briefly describe them in turn in the following subsections.

### 2.1 The LHC-like new physics search Likelihood

As a first example we consider the toy LHC-like NP search, here after referred as the Toy Likelihood, introduced in Ref. [13] and also considered in Ref. [1]. We refer the reader to

<sup>1</sup>We are aware of an upcoming paper proposing a similar approach in a different context [12].

those references for a detailed explanation of the Likelihood construction, its parameters, and its sampling. Here we limit ourselves to remind that the Likelihood depends on one signal strength parameter  $\mu$  and 94 nuisance parameters  $\delta$ .

## 2.2 The ElectroWeak fit Likelihood

The second Likelihood we consider is the one corresponding to the ElectroWeak fit presented in Ref. [14], which includes the recent top quark mass measurement by the CMS Collaboration [15] and  $W$  boson mass measurement by the CDF Collaboration [16]. Such Likelihood, that we call EW Likelihood, depends on 40 parameters: 32 nuisance parameters and 8 parameters of interest, corresponding to the Wilson coefficients of the relevant Standard Model Effective Field Theory (SMEFT) operators. A sampling of the posterior probability distribution has been obtained with the HEPFit code [17]. The complete list of parameters with their definitions is reported in Appendix A.

In this case, the 1D marginal distributions of the parameters are all nearly Gaussian, with the exception of two truncated Gaussians, so that we expect it to be relatively simple for a NF with a Gaussian base distribution to learn the posterior. Nevertheless, the posterior shows strong correlations among some pairs of parameters (see Figure 5 in Appendix A), which helps to understand the ability of the NFs to accurately learn the correlation matrix.

## 2.3 The Flavor fit Likelihood

The third Likelihood we consider corresponds to the EFT fit to flavor observables related to neutral current  $b \rightarrow s$  transitions presented in Ref. [18]. This Likelihood, refereed to as the Flavor Likelihood, depends on 89 parameters: 77 nuisance parameters and 12 parameters of interest, corresponding to the Wilson coefficients of the relevant SMEFT operators. A sampling of the posterior probability distribution has been obtained with the HEPFit code documented in Ref. [17]. The full list of parameters is reported in Appendix A. This Likelihood is clearly more complicated than the previous two, since it features multimodal 1D distributions and complicated correlations (see Figs 3 and 4).

## 3 Evaluation Metrics

We used as quality metrics the mean over dimensions of the  $p$ -values of 1D Kolmogorov-Smirnov test (KS-test), with an optimal value of 0.5 and the Sliced Wasserstien distance (SWD) [19, 20], with optimal value 0. We briefly recall their definitions here for convenience:

- **Kolmogorov-Smirnov Test (KS)**

The Kolmogorov-Smirnov (KS) test serves as a statistical test for assessing if two one-dimensional samples originate from the same underlying (unknown) probability density function (PDF). The null hypothesis assumes that both sets of samples are derived from the same PDF. The KS metric can be expressed as:

$$D_{y,z} = \sup_x |F_y(x) - F_z(x)|, \quad (1)$$

where  $F_{y,z}(x)$  is the empirical cumulative distribution functions of the sample sets  $\{y_i\}$  and  $\{z_i\}$ , while  $\sup$  denotes the supremum function. The  $p$ -value for null hy-

pothesis rejection is given by:

$$D_{y,z} > \sqrt{-\ln\left(\frac{p}{2}\right) \times \frac{1 + \frac{n_z}{n_y}}{2n_z}} \quad (2)$$

where  $n_y$  and  $n_z$  indicate the sample sizes.

- **Sliced Wasserstein Distance (SWD)**

The SWD serves as a metric for comparing two multi-dimensional distributions, leveraging the one-dimensional Wasserstein distance. The one-dimensional Wasserstein distance between two empirical distributions is formulated as:

$$W_{y,z} = \int_{\mathbb{R}} dx |F_y(x) - F_z(x)| \quad (3)$$

In our sliced approach, we randomly select  $N_d = 2D$  directions, with  $D$  the dimensionality of the sample, uniformly distributed over the  $4\pi$  solid angle.<sup>2</sup> We then project all samples on such directions and compute the one-dimensional Wasserstein distance and finally take the mean over the directions.

In order to include statistical uncertainty on the test and NF generated samples we compute the above metrics 100 times, for independent batches of  $N_{\text{test}}/100$  points, and take the average.

With respect to the Ref. [3] we also consider here the metric given by the discrepancy on the Highest Posterior Density Interval (HPDI). This is a very important metric for Bayesian posterior inference, since it tells how well credibility intervals (CI) are reproduced by the NFLikelihood. In particular, we computed the HPDI relative error width (HPDIe) for 68.27%, 95.45%, and 99.73% (CI) of each 1D marginal of the true and predicted distributions. For each dimension, we compute the mean of this quantity when more than one interval is present (which is common for multimodal distributions). Finally, we take the median over all dimensions. We choose the median to avoid that results on very noisy dimensions, particularly in the Flavor Likelihood, have a large negative effect on the generally good value of the metric.

## 4 The NFLikelihood

The results of this analysis have been obtained using the TensorFlow2 NF implementation from Ref. [3]. The Toy Likelihood was trained with a Masked Autoregressive Flow (MAF) architecture [22], while the EW and Flavor Likelihoods were trained with an Autoregressive Rational Quadratic Spline (A-RQS) architecture [23], always training with a log-probability loss function. For all three cases the training data was always standardized (to zero mean and unit standard deviation) before training and a small scan over the flow's hyperparameters was performed. Here we only present the optimal results obtained for each distribution. All training iterations were performed with an initial learning rate of 0.001, reduced by a factor of 0.2 after a *patience* number of epochs without improvement on the validation loss. Training was early stopped after  $2 \cdot \textit{patience}$  number of epochs without improvement. The value of *patience* and of the other relevant hyperparameters will be reported separately for each of the Likelihoods. All models have been trained on Tesla V100 Nvidia GPUs.

<sup>2</sup>This is achieved by normalizing an  $N$ -dimensional vector whose components are sampled from independent standard normal distributions [21].



Hyperparameters for Toy Likelihood								
# of samples	hidden layers	# of bijec.	algorithm	spline knots	range	L1 factor	patience	max # of epochs
$2 \cdot 10^5$	$3 \times 64$	MAF	2	-	-	0	20	200

Table 1: Hyperparameters leading to the best determination of the Toy Likelihood.

Results for Toy Likelihood						
# of samples	Mean KS-test	Mean SWD	HPDI $e_{1\sigma}$	HPDI $e_{2\sigma}$	HPDI $e_{3\sigma}$	time (s)
$2 \cdot 10^5$	0.4893	0.03947	0.02073	0.01207	0.01623	133

Table 2: Best results obtained for the Toy Likelihood.

Results for Toy Likelihood POI				
POI	KS-test	HPDI $e_{1\sigma}$	HPDI $e_{2\sigma}$	HPDI $e_{3\sigma}$
$\mu$	0.54	0.02742	0.01359	0.01786

Table 3: Best results POI flavor.

#### 4.1 The Toy Likelihood

The hyperparameters that lead to the best estimation of the Toy Likelihood are shown in Table 1. The corresponding NF architecture is made of two MAF bijectors and one reverse permutation between them. Each MAF has an autoregressive network with 3 hidden layers made of 64 nodes each. The training was performed for a maximum of 200 epochs, with *patience* = 20 and  $2 \cdot 10^5$  training samples. The NF model was tested with  $2 \cdot 10^5$  test samples.

The resulting quality metrics are shown in Table 2. In particular, we obtained an optimal KS-test of  $\sim 0.5$  and HPDI $e$  of the order of  $10^{-2}$ , which guarantee that, within the considered statistical uncertainty, the NF generated samples are indistinguishable from those generated with the true pdf. The training time was about 300s. Since, when doing inference from a Likelihood function or posterior distribution, one is usually specially interested in the so-called parameters of interests (POIs), we show in Table 3 the results obtained for  $\mu$ . Here the KS-test is again  $\sim 0.5$  and HPDI $e$ s of the order of  $10^{-2}$ . The accuracy of the NF model is visually shown in Figure 1, which presents a corner plot of a selection of 10 parameters, including  $\mu$ . In the Figure, the true distribution is shown in red, while the NF distribution in blue. The HPDI $e$ s corresponding to 68.27% ( $1\sigma$ ), 95.45% ( $2\sigma$ ), and 99.73% ( $3\sigma$ ) probabilities are shown as solid, dashed and dashed-dotted lines, respectively. The selected parameters include those considered in Ref. [1], therefore allowing for a direct comparison. In particular, comparing with what in Ref. [1] is called the Bayesian DNNLikelihood, we find that both approaches gives extremely accurate results: the NF approach seems to perform slightly better, even though the DNNLikelihood was trained with half the number of training points of the NFLikelihood ( $10^5$ ). The main difference seems to be in the training time, which is much larger for the DNNLikelihood. The advantage of the DNNLikelihood with respect to the NFLikelihood comes when the so-called Frequentist Likelihood is considered: in this case one is not particularly interested in learning the Likelihood (or the posterior) as a PDF, but is instead interested in learning it as a function close to its absolute and local (profiled) maxima. This highlights the main difference between the DNNLikelihood and the NFLikelihood. The first is more suitable to encode Likelihoods to be used for frequentist analyses, while the second for Likelihoods

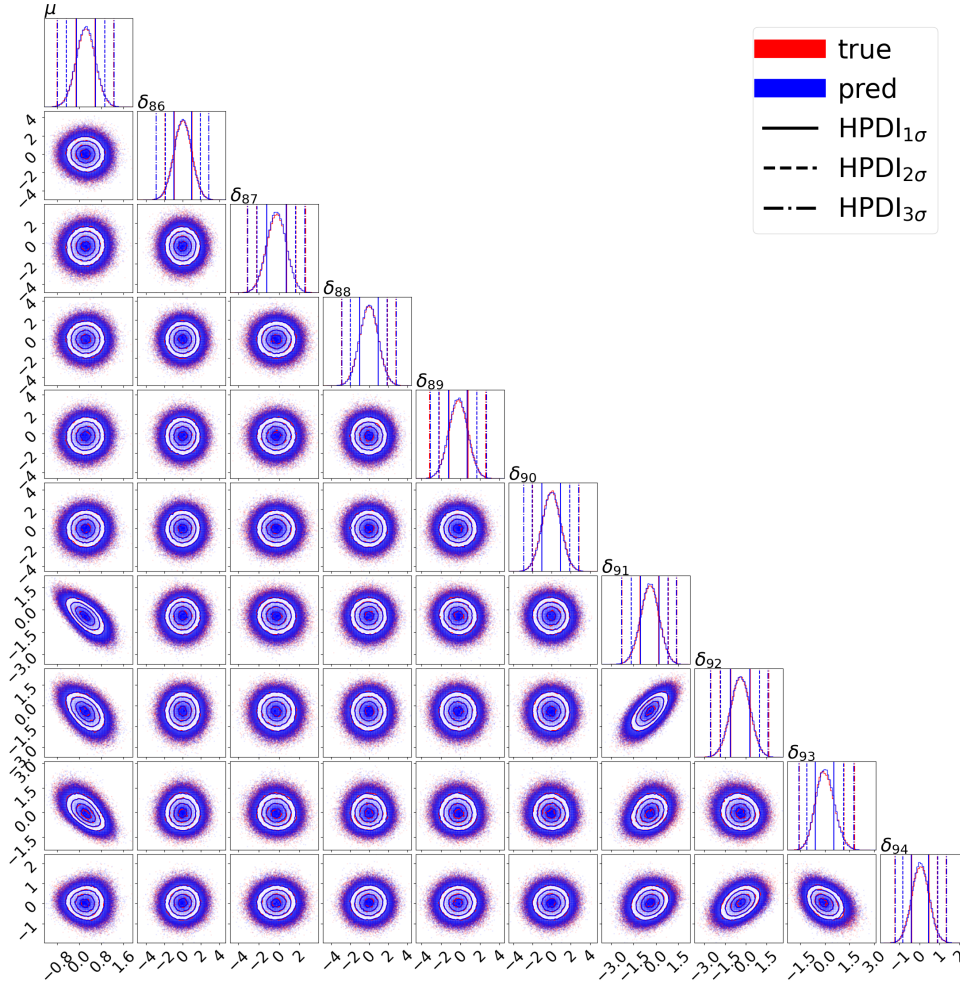


Figure 1: Corner plot of the 1D and 2D marginal posterior distributions of a representative selection of the Toy Likelihood parameters. The true distribution is depicted in red, while the predicted distribution is shown in blue. The solid, dashed and dashed-dotted line over the 1D marginals denote the 68.27%, 95.45%, and 99.73% HPDIs, respectively. The rings on the 2D marginals describe the corresponding probability levels.

(or posteriors) to be used in Bayesian analyses. Obviously one can combine the two approaches to obtain a general and flexible representation of the Likelihood suitable for both frequentist and Bayesian inference. We defer this generalization to future work.

## 4.2 The EW Likelihood.

The hyperparameters corresponding to the best NF model describing the EW Likelihood are shown in Table 4. The chosen NF architecture is made of two A-RQS bijectors with 4 spline knots defined in a  $[-6, 6]$  range, and one reverse permutation between them. Each A-RQS has an autoregressive network with 3 hidden layers made of 128 nodes each. The training was performed for a maximum of 800 epochs and a patience of 20 with  $2 \cdot 10^5$  training samples. The NF model was tested with  $2 \cdot 10^5$  samples. Finally, given the presence of truncated dimensions, the distributions were soft clipped, with a hinge factor of  $10^{-4}$  at the truncations, within the range of the training data.

A summary of the values obtained for the evaluation metrics is reported in Table 5. We obtained a mean KS-test of  $\sim 0.4$  and HPDIes of the order of  $10^{-3}$  or smaller. The training time was about 7200 s, that is a couple of hours. Furthermore, Table 3 shows the

Hyperparameters for the EW Likelihood								
# of samples	hidden layers	# of bijec.	algorithm	spline knots	range	L1 factor	patience	# of epochs
$2 \cdot 10^5$	2	$3 \times 128$	A-RQS	4	-6	0	20	800

Table 4: Hyperparameters leading to the best determination of the EW Likelihood.

Results for the EW Likelihood						
# of samples	Mean KS-test	Mean SWD	HPDLe <sub>1σ</sub>	HPDLe <sub>2σ</sub>	HPDLe <sub>3σ</sub>	time (s)
$2 \cdot 10^5$	0.4269	0.003066	0.0006896	0.0006578	0.006181	7255

Table 5: Best results obtained on the EW Likelihood.

Results for EW Likelihood					
POI	KS-test	HPDLe <sub>1σ</sub>	HPDLe <sub>2σ</sub>	HPDLe <sub>3σ</sub>	
$c_{\varphi l}^1$	0.2089	0.05913	0.09649	0.2618	
$c_{\varphi l}^3$	0.2224	0.03072	0.1328	0.5699	
$c_{\varphi q}^1$	0.4308	0.03586	0.01308	0.03996	
$c_{\varphi q}^3$	0.4612	0.008389	0.03182	2.8446	
$c_{\varphi d}$	0.4478	0.0008574	0.04543	0.1011	
$c_{\varphi e}$	0.4831	0.01389	0.1226	0.1393	
$c_{\varphi u}$	0.4847	0.02874	0.006302	0.2268	
$c_{ll}$	0.2574	0.1487	0.0868	0.06874	

Table 6: Results for the Wilson coefficients in the EW Likelihood.

metrics obtained for the Wilson coefficients (POIs). We find that the POIs are generally well described, albeit some small deviations after  $2\sigma$  interval, which can be likely fixed after further fine-tuning the hyperparameters or adding more training points.

The true and NF distributions are visually compared in Figure 2, which shows a corner plot over the POIs plus four representative nuisance parameters (a total of twelve parameters). As before, the distribution is represented in red, while the NF distribution in blue. The HPDIs corresponding to 68.27%, 95.45%, and 99.73% probabilities are shown as solid, dashed and dashed-dotted lines, respectively. We see that in general, the NF distributions matches pretty well the true one. Something worth emphasizing is the NF ability to learn even large correlations between dimensions. This is not expected in the case of the DNNLikelihood, since regression becomes inefficient when large correlations between parameters are present.

### 4.3 Flavor Likelihood

The optimal hyperparameters found for learning the Flavor Likelihood are shown in Table 7. The chosen NF architecture is made of two A-RQS bijectors with 8 spline knots defined in the  $[-5, 5]$  range, and one reverse permutation between them. Each A-RQS has an autoregressive network with 3 hidden layers made of 1024 nodes each and an L1 regularization factor of  $10^{-4}$ . The training was performed for a maximum of 12000 epochs with a patience of 50. The model was trained with  $10^6$  samples and tested with  $5 \cdot 10^5$  samples. Furthermore, since the Likelihood function presents several truncated dimensions, the NF



Hyperparameters for the Flavor Likelihood								
# of samples	hidden layers	# of bijec.	algorithm	spline knots	range	L1 factor	patience	max # of epochs
$10^6$	$3 \times 1024$	2	A-RQS	8	-5	1e-4	50	12000

Table 7: Hyperparameters leading to the best determination of the Flavor Likelihood.

Results for the Flavor Likelihood						
# of samples	Mean KS-test	Mean SWD	HPD $I_{e1\sigma}$	HPD $I_{e2\sigma}$	HPD $I_{e3\sigma}$	time (s)
$10^6$	0.3163	0.04031	0.01154	0.01354	1.738e-5	9550

Table 8: Best results obtained for the Flavor Likelihood.

Results for Flavor Likelihood POIs					
POI	KS-test	HPD $I_{e1\sigma}$	HPD $I_{e2\sigma}$	HPD $I_{e3\sigma}$	
$c_{1123}^{LQ1}$	0.2056	0.1488	7.6285	4.731e-08	
$c_{2223}^{LQ1}$	0.316	0.008596	0.009739	0.03413	
$c_{1123}^{Ld}$	0.4626	0.02686	0.01354	0.03553	
$c_{2223}^{Ld}$	0.239	0.06724	0.01053	2.398e-08	
$c_{11}^{LedQ}$	0.3585	0.05904	0.01171	5.387e-08	
$c_{22}^{LedQ}$	0.3474	0.02035	0.008888	2.155e-09	
$c_{2311}^{Qe}$	0.2761	0.01753	0.01449	1.419e-07	
$c_{2322}^{Qe}$	0.1362	0.05067	0.03221	0.009614	
$c_{1123}^{ed}$	0.4518	0.02477	0.005794	5.602e-08	
$c_{2223}^{ed}$	0.3939	0.007526	0.01198	1.502e-08	
$c_{11}'^{LedQ}$	0.4603	0.007353	0.01401	8.011e-08	
$c_{22}'^{LedQ}$	0.4385	1.8112	0.007142	4.374e-08	

Table 9: Results for the Wilson coefficients in the Flavor Likelihood.

complex correlations and noisy dimensions, offering a very realistic prototype of a complicated high dimensional HEP Likelihood. Nonetheless, we find that the NF model is able to reproduce it with a very good accuracy.

## 5 Conclusion

The publication of full Likelihoods is crucial for the long lasting legacy of the LHC, and for any other experiment involving complicated analyses with a large parameter space. However, this is not always a straightforward matter since Likelihoods are often high dimensional complex distributions, sometimes depending on Monte Carlo simulations and/or numeric integrations, which make their sampling a very hard task. Furthermore, one requires precise, compact, and efficient representations of them so that they can be easily and systematically reused. As it was first shown in Ref. [1], Neural Networks, being universal interpolators, offer a promising approach to encode, preserve, and reuse Likelihood functions. In this work we extended this approach to unsupervised learning, proposing



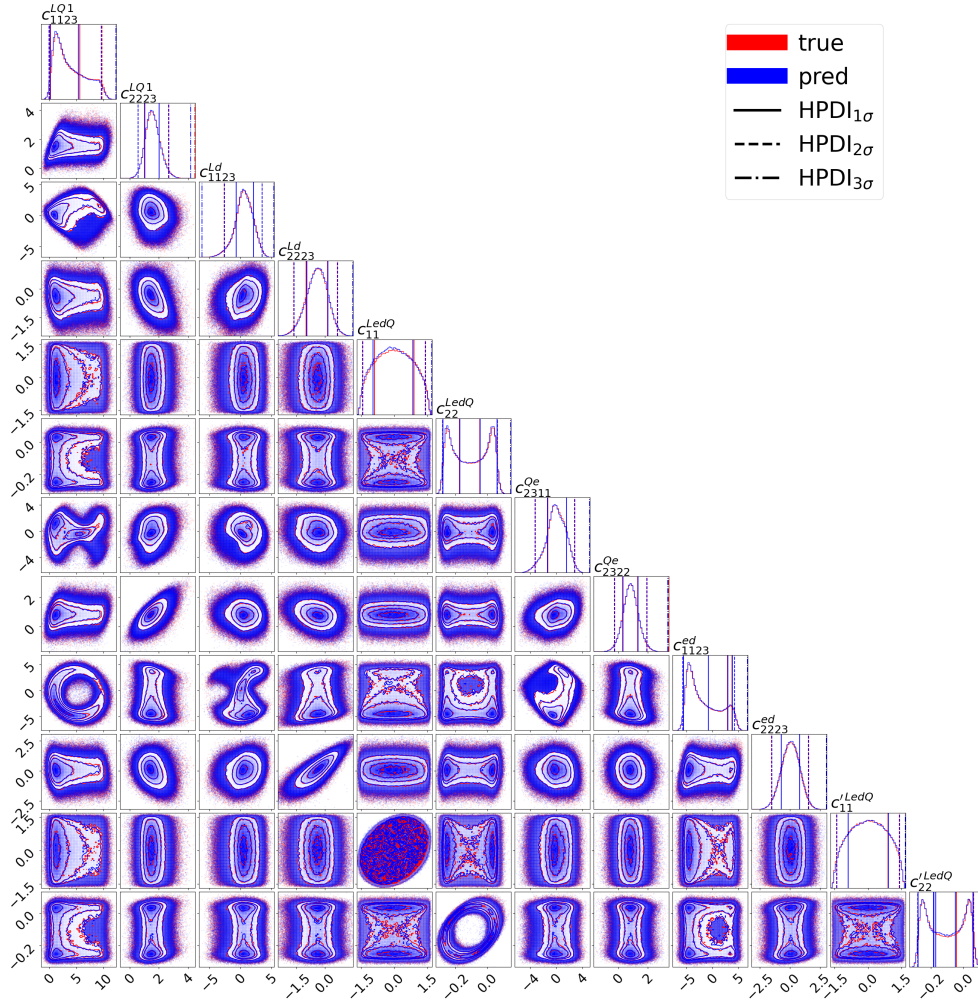


Figure 3: Corner plot of the 1D and 2D marginal posterior distributions of the Wilson coefficients of the Flavor Likelihood. The true distribution is depicted in red, while the predicted distribution is shown in blue. The solid, dashed and dashed-dotted line over the 1D marginals denote the 68.27%, 95.45%, and 99.73% HPDIs, respectively. The rings on the 2D marginals describe the corresponding probability levels.

the use of Normalizing Flows for this endeavor. Indeed, Normalizing Flows are powerful generative models which, by construction, also provide density estimation. We tested our proposal on three posterior distributions of increasing complexity, corresponding to three different Likelihood functions: a 95-dimensional LHC-like new physics search Likelihood, a 40-dimensional ElectroWeak EFT fit Likelihood, and an 89-dimensional Flavor EFT fit Likelihood. We found that Autoregressive Normalizing Flows are capable of precisely describing all the above examples, including all the multimodalities, truncations, and complicated correlations. In fact, we see that, given the way they are constructed, Autoregressive Flows can easily learn the covariance matrices of the distributions. Both the code used for this project [24] and a user-friendly TENSORFLOW2 framework for Normalizing Flows (still under development) [25] are available on GitHub. The training and generated data, as well as the trained NF models, are available on Zenodo [26].

The 95-dimensional LHC-like new physics search Likelihood, which was also studied in the context of the DNNLikelihood of Ref. [1] was also used to make a comparison between the two approaches. Such comparison leads to the conclusion that the two approaches are complementary and could, in the future, be merged to get an even more flexible





#	Parameter	Description	#	Parameter	Description
1	$\alpha_S(M_Z)$	SM input	21	$C_{\varphi u}$	Wilson coefficient
2	$\Delta\alpha_{\text{had}}^{(5)}(M_Z)$	SM input	22	$C_{ll}$	Wilson coefficient
3	$M_Z$	SM input	23	$P_{\tau}^{\text{pol}}$	Observable
4	$m_H$	SM input	24	$M_W$	Observable
5	$m_t$	SM input	25	$\Gamma_W$	Observable
6	$\delta_{\Gamma_Z}$	SM input uncertainty	26	$\text{BR}_{W \rightarrow l\bar{\nu}_l}$	Observable
7	$\delta_{M_W}$	SM input uncertainty	27	$\mathcal{A}_s$	Observable
8	$\delta_{R_b^0}$	SM input uncertainty	28	$R_{uc}$	Observable
9	$\delta_{R_c^0}$	SM input uncertainty	29	$\sin^2 \theta_{\text{eff}}$	Observable
10	$\delta_{R_l^0}$	SM input uncertainty	30	$\Gamma_Z$	Observable
11	$\delta_{\sin^2 \theta_{\text{eff}^b}}$	SM input uncertainty	31	$\sigma_h^0$	Observable
12	$\delta_{\sin^2 \theta_{\text{eff}^t}}$	SM input uncertainty	32	$R_l^0$	Observable
13	$\delta_{\sin^2 \theta_{\text{eff}^q}}$	SM input uncertainty	33	$A_{\text{FB}}^{0,l}$	Observable
14	$\delta_{\sigma_h^0}$	SM input uncertainty	34	$\mathcal{A}_l$	Observable
15	$C_{\varphi l}^1$	Wilson coefficient	35	$R_b^0$	Observable
16	$C_{\varphi l}^3$	Wilson coefficient	36	$R_c^0$	Observable
17	$C_{\varphi q}^1$	Wilson coefficient	37	$A_{\text{FB}}^{0,b}$	Observable
18	$C_{\varphi q}^3$	Wilson coefficient	38	$A_{\text{FB}}^{0,c}$	Observable
19	$C_{\varphi d}$	Wilson coefficient	39	$\mathcal{A}_b$	Observable
20	$C_{\varphi e}$	Wilson coefficient	40	$\mathcal{A}_c$	Observable

Table 10: Parameters of the EW Likelihood.

## A Details of the EW and Flavor Likelihoods

The list of parameters and their description for the EW Likelihood is given in Table 10, while Figure 5 gives a pictorial representation of the data correlation matrix. The list of parameters and their description for the Flavor Likelihood is given in Table 11.

## References



- [1] A. Coccaro, M. Pierini, L. Silvestrini and R. Torre, “*The DNNLikelihood: enhancing likelihood distribution with Deep Learning*”, *Eur.Phys.J.C* **80** (2020) 664, [arXiv:1911.03305](#) [SEMANTIC SCHOLAR].
- [2] K. Cranmer et al., “*Publishing statistical models: Getting the most out of particle physics experiments*”, *SciPost Phys.* **12** (2022) 037, [arXiv:2109.04981](#) [SEMANTIC SCHOLAR].
- [3] A. Coccaro, M. Letizia, H. Reyes-Gonzalez and R. Torre, “*On the curse of dimensionality for Normalizing Flows*”, [arXiv:2302.12024](#) [SEMANTIC SCHOLAR].
- [4] S. S. Gu, Z. Ghahramani and R. E. Turner, “*Neural Adaptive Sequential Monte Carlo*”, in *Advances in Neural Information Processing Systems*, C. Cortes, N. Lawrence, D. Lee, M. Sugiyama and R. Garnett, eds., vol. 28, Curran Associates, Inc., 2015, [arXiv:1506.03338](#) [SEMANTIC SCHOLAR].



Table 11: Parameters of the Flavor Likelihood

#	Parameter	Description	#	Parameter	Description	#	Parameter	Description
1	$ h_0^{(0)} $	Nuis	31	$a_0^{A0}$	Nuis	61	$a_{1\phi}^V$	Nuis
2	$ h_+^{(0)} $	Nuis	32	$a_0^{A1}$	Nuis	62	$a_{2\phi}^{A0}$	Nuis
3	$ h_-^{(0)} $	Nuis	33	$a_0^{T1}$	Nuis	63	$a_{2\phi}^{A1}$	Nuis
4	$\arg(h_0^{(0)})$	Nuis	34	$a_0^{T23}$	Nuis	64	$a_{2\phi}^{A12}$	Nuis
5	$\arg(h_+^{(0)})$	Nuis	35	$a_0^V$	Nuis	65	$a_{2\phi}^{T1}$	Nuis
6	$\arg(h_-^{(0)})$	Nuis	36	$a_1^{A0}$	Nuis	66	$a_{2\phi}^{T2}$	Nuis
7	$ h_0^{(1)} $	Nuis	37	$a_1^{A1}$	Nuis	67	$a_{2\phi}^{T23}$	Nuis
8	$ h_+^{(1)} $	Nuis	38	$a_1^{A12}$	Nuis	68	$a_{2\phi}^V$	Nuis
9	$ h_-^{(1)} $	Nuis	39	$a_1^{T1}$	Nuis	69	$b_0 f_0$	Nuis
10	$\arg(h_0^{(1)})$	Nuis	40	$a_1^{T2}$	Nuis	70	$b_0 f_T$	Nuis
11	$\arg(h_+^{(1)})$	Nuis	41	$a_1^{T23}$	Nuis	71	$b_0 f_+$	Nuis
12	$\arg(h_-^{(1)})$	Nuis	42	$a_1^V$	Nuis	72	$b_1 f_0$	Nuis
13	$ h_+^{(2)} $	Nuis	43	$a_2^{A0}$	Nuis	73	$b_1 f_T$	Nuis
14	$ h_-^{(2)} $	Nuis	44	$a_2^{A1}$	Nuis	74	$b_1 f_+$	Nuis
15	$\arg(h_+^{(2)})$	Nuis	45	$a_2^{A12}$	Nuis	75	$b_2 f_0$	Nuis
16	$\arg(h_-^{(2)})$	Nuis	46	$a_2^{T1}$	Nuis	76	$b_2 f_T$	Nuis
17	$ h_0^{(MP)} $	Nuis	47	$a_2^{T2}$	Nuis	77	$b_2 f_+$	Nuis
18	$\arg(h_0^{(MP)})$	Nuis	48	$a_2^{T23}$	Nuis	78	$c_{1123}^{LQ1}$	Wilson coefficient
19	$ h_1^{(MP)} $	Nuis	49	$a_2^V$	Nuis	79	$c_{2223}^{LQ1}$	Wilson coefficient
20	$\arg(h_1^{(MP)})$	Nuis	50	$a_{0\phi}^{A0}$	Nuis	80	$c_{1123}^{Ld}$	Wilson coefficient
21	$ h_2^{(MP)} $	Nuis	51	$a_{0\phi}^{A1}$	Nuis	81	$c_{2223}^{Ld}$	Wilson coefficient
22	$\arg(h_1^{(MP)})$	Nuis	52	$a_{0\phi}^{T1}$	Nuis	82	$c_{11}^{LedQ}$	Wilson coefficient
23	$F_{Bs}/F_{Bd}$	Nuis	53	$a_{0\phi}^{T23}$	Nuis	83	$c_{22}^{LedQ}$	Wilson coefficient
24	$\delta G_{Gs}$	Nuis	54	$a_{0\phi}^V$	Nuis	84	$c_{2311}^{Qe}$	Wilson coefficient
25	$F_{Bs}$	Nuis	55	$a_{1\phi}^{A0}$	Nuis	85	$c_{2322}^{Qe}$	Wilson coefficient
26	$\lambda_B$	Nuis	56	$a_{1\phi}^{A1}$	Nuis	86	$c_{1123}^{ed}$	Wilson coefficient
27	$\alpha_1(K^*)$	Nuis	57	$a_{1\phi}^{A12}$	Nuis	87	$c_{2223}^{ed}$	Wilson coefficient
28	$\alpha_2(K^*)$	Nuis	58	$a_{1\phi}^{T1}$	Nuis	88	$c_{11}^{JLedQ}$	Wilson coefficient
29	$\alpha_2(\phi)$	Nuis	59	$a_{1\phi}^{T2}$	Nuis	89	$c_{22}^{JLedQ}$	Wilson coefficient
30	$\alpha_1(K')$	Nuis	60	$a_{1\phi}^{T23}$	Nuis			

- [11] K. Cranmer, G. Kanwar, S. Racanière, D. J. Rezende and P. Shanahan, “*Advances in machine-learning-based sampling motivated by lattice quantum chromodynamics*”, *Nature Rev. Phys.* **5** (2023) 526, [arXiv:2309.01156](#) [SEMANTIC SCHOLAR].
- [12] A. Beck, M. Reboud and D. van Dyk, “*Testable likelihoods for beyond-the-standard model fits*”, To appear.
- [13] A. Buckley, M. Citron, S. Fichet, S. Kraml, W. Waltenberger and N. Wardle, “*The Simplified Likelihood Framework*”, *JHEP* **04** (2019) 064, [arXiv:1809.05548](#) [SEMANTIC SCHOLAR].
- [14] J. de Blas, M. Pierini, L. Reina and L. Silvestrini, “*Impact of the recent measurements of the top-quark and W-boson masses on electroweak precision fits*”, *Phys. Rev. Lett.* **129** (2022) 271801, [arXiv:2204.04204](#) [SEMANTIC SCHOLAR].
- [15] CMS Collaboration, “*Measurement of the top quark mass using a profile likelihood approach with the lepton+jets final states in proton-proton collisions  $\sqrt{s} = 13$  TeV*”, [arXiv:2302.01967](#) [SEMANTIC SCHOLAR].

- [16] CDF Collaboration, T. Aaltonen et al., “*High-precision measurement of the  $W$  boson mass with the CDF II detector*”, *Science* **376** (2022) 170 [SEMANTIC SCHOLAR].
- [17] J. De Blas et al., “*HEPfit: a code for the combination of indirect and direct constraints on high energy physics models*”, *Eur. Phys. J. C* **80** (2020) 456, [arXiv:1910.14012](#) [SEMANTIC SCHOLAR].
- [18] M. Ciuchini, A. M. Coutinho, M. Fedele, E. Franco, A. Paul, L. Silvestrini et al., “*New Physics in  $b \rightarrow s\ell^+\ell^-$  confronts new data on Lepton Universality*”, *Eur. Phys. J. C* **79** (2019) 719, [arXiv:1903.09632](#) [SEMANTIC SCHOLAR].
- [19] J. Rabin, G. Peyré, J. Delon and M. Bernot, “*Wasserstein Barycenter and Its Application to Texture Mixing*”, in *Scale Space and Variational Methods in Computer Vision*, A. M. Bruckstein, B. M. ter Haar Romeny, A. M. Bronstein and M. M. Bronstein, eds., pp. 435–446, Springer Berlin Heidelberg, Berlin, Heidelberg, 2012 [SEMANTIC SCHOLAR].
- [20] N. Bonneel, J. Rabin, G. Peyré and H. Pfister, “*Sliced and Radon Wasserstein Barycenters of Measures*”, *Journal of Mathematical Imaging and Vision* **51** (2015) 22 [SEMANTIC SCHOLAR].
- [21] M. E. Muller, “*A note on a method for generating points uniformly on  $n$ -dimensional spheres*”, *Commun. ACM* **2** (1959) 19–20 [SEMANTIC SCHOLAR].
- [22] G. Papamakarios, T. Pavlakou and I. Murray, “*Masked Autoregressive Flow for Density Estimation*”, in *Advances in Neural Information Processing Systems*, I. Guyon, U. V. Luxburg, S. Bengio, H. Wallach, R. Fergus, S. Vishwanathan et al., eds., vol. 30, Curran Associates, Inc., 2017, [arXiv:1705.07057](#) [SEMANTIC SCHOLAR].
- [23] C. Durkan, A. Bekasov, I. Murray and G. Papamakarios, “*Neural Spline Flows*”, in *Proceedings of the 33rd International Conference on Neural Information Processing Systems*, Curran Associates Inc., Red Hook, NY, USA, 2019, [arXiv:1906.04032](#) [SEMANTIC SCHOLAR].
- [24] Code repository for this paper on GITHUB .
- [25] NF4HEP code repository on GITHUB .
- [26] Data repository for this paper on ZENODO [ZENODO](#).
- [27] C. Winkler, D. Worrall, E. Hoozeboom and M. Welling, “*Learning likelihoods with conditional normalizing flows*”, [arXiv:1912.00042](#) [SEMANTIC SCHOLAR].